Desalination and Water Treatment
www.deswater.com

doi: 10.5004/dwt.2019.24433

164 (2019) 215–227
October

Metronidazole adsorption on $CoFe_2O_4$/activated carbon@chitosan as a new magnetic biocomposite: modelling, analysis, and optimization by response surface methodology

Mohammad Malakootian[a,b], Alireza Nasiri[a], Hakimeh Mahdizadeh[b,*]

[a]*Environmental Health Engineering Research Center, Kerman University of Medical Sciences, Kerman, Iran, email: m.malakootian@yahoo.com (M. Malakootian), nasiri.kmu@gmail.com (A. Nasiri)*
[b]*Department of Environmental Health, School of Public Health, Kerman University of Medical Sciences, Kerman, Iran Phone: +98 343 132 5128, Fax +98 343 132 5435, email: H.Mahdizadeh2018@gmail.com (H. Mahdizadeh)*

Received 23 December 2018; Accepted 19 May 2019

ABSTRACT

A novel magnetic biocomposite adsorbent $CoFe_2O_4$/Activated Carbon@Chitosan (CF/AC@Ch) was synthesized and applied for metronidazole (MNZ) adsorption from aqueous solutions. The magnetic biocomposite adsorbent was characterized by field emission scanning electron microscopy (FESEM), the Brunauer–Emmett–Teller (S_{BET}), Fourier transform infrared spectroscopy (FTIR), X-ray powder diffraction (XRD), and vibrating sample magnetometer (VSM). Powder XRD analysis confirmed the formation of phase spinel ferrites. FESEM analysis confirmed the morphology of the samples with a smaller agglomeration. VSM analysis clearly showed the ferromagnetic nature of the adsorbent. The Ms value was 22.03 emu/g for simple separation by external magnetic fields. The influence of parameters such as the adsorbent dose, pH, MNZ initial concentration, and contact time was examined and evaluated by central composite design (CCD) with response surface methodology (RSM). The predicted optimal adsorption capacity (q_e) of 36.897 mg/g was obtained under optimal conditions as follows; adsorbent dose: 450 mg/L, pH: 5.02, MNZ initial concentration: 22.35 mg/L and contact time: 46.25 min. The quadratic model was obtained with a high degree of fit. The experimental equilibrium data fitting to Langmuir and Freundlich models show that the Freundlich model is a good and suitable model for evaluation and the actual behavior of adsorption. The equilibrium adsorption capacity of MNZ declined from 35.90 mg/g in the pure solution of MNZ to 21.5 mg/g in the wastewater sample.

Keywords: Metronidazole; Optimization; Magnetic biocomposite; Response surface methodology

1. Introduction

Discharge of antibiotics to the aquatic environment exhibits detrimental effects on the aquatic ecosystem and humans, such as drug resistance in humans and animals, alteration of the algae structure in aquatic systems and effect on non-target pathogens [1]. Metronidazole (MNZ) is a type of nitroimidazole antibiotic, which is commonly used for the treatment of infectious diseases caused by anaerobic bacteria and protozoans, such as *Trichomonas vaginalis* and *Giardia lamblia Giardia*. Recently, MNZ has been detected in hospital effluents at concentration levels of µg/L to mg/L. Therefore, MNZs are potentially hazardous compounds that have low biodegradability and are resistant in the environment [2–4]. Although their concentrations may be low in these environments, they can accumulate in the food chain and increase concerns about adverse effects associated with them. Therefore, the removal of antibiotics from aquatic systems is vital [5].

---

*Corresponding author.

The processes used for antibiotics removal from aqueous solutions include coagulation and flocculation, chemical oxidation, biological treatment, electrochemical techniques, ion exchange, and adsorption [4–9]. These methods, however, have some disadvantages. For instance, the removal of sustainable pollutants in biological systems also takes place slowly and under particular biological conditions [3,8,10]. Moreover, the high consumption of chemicals and creation of secondary pollution by the addition of chemical compounds are also among the disadvantages of chemical oxidation methods [8,10]. Therefore, the use of most of these techniques is not practical in the industry. Among these methods, the adsorption process is widely used in water and wastewater treatment plants because of its low energy and maintenance costs, simplicity and reliability [11,12].

Up to now, numerous materials have been synthesized and reported in literatures for the treatment of water and wastewater as adsorbents, catalysts and resins, including magnetic biochar supported g-C_3N_4/$FeVO_4$ [13], biopolymer based nanohydrogels [14,15], *Hibiscus cannabinus* fibers [16], alizarin red-S-loaded amberlite IRA-400 resins [17], biochar-templated g-C_3N_4/$Bi_2O_2CO_3$/$CoFe_2O_4$ nano-assembly [18], starch/SnO_2 nanocomposites [19], gum arabic-*cl* poly(acrylamide) nanohydrogels [20], surfactant assisted nano-composite cation exchangers [21], pectin based quaternary amino anion exchangers [22], cross-linked chitosan/sepiolite composites [23], cross-linked beads of activated oil palm ash zeolite/chitosan composites [24], mesoporous-activated carbons [25], large surface area date stone activated carbons [26], etc.

The use of natural and bio-based materials (organic or inorganic) as bioadsorbents due to their high biodegradability as well as their high gelling and stabilizing nature has received a great deal of attention [14,19,22]. The main limitation in using powdered activated carbons or other adsorbents with nano size particles is the difficulty for separating them, filtering them from solutions and creating turbidity due to the small size of particles [27–29]. During recent years, there has been much interest in novel adsorbents to remove pollutants from aquatic environments [30,31]. Cobalt ferrite ($CoFe_2O_4$) is a well-known hard magnetic material with high electromagnetic performance, excellent chemical stability, mechanical hardness, high coercivity, and moderate saturation magnetization (Ms) [32].

Modification of magnetic adsorbents with organic materials or inorganic materials such as biopolymers, biomolecules, pectin, cellulose, alginate, chitosan, gurgum silica, metals, etc. can improve the adsorbing capabilities of magnetic nanoparticles in wastewater [19,22,33]. Chitosan is considered to be one of the most promising and applicable adsorbents due to its high reactivity, high chelation and high selectivity for various pollutants, and thus is useful as a bio-adsorbent to remove pollutants from aqueous solutions [13,33].

Conventionally, optimization of batch mode studies has been carried out using a traditional one-variable-at-a-time approach. However, this technique completely fails to represent the effects of interaction among variables and also it is time consuming and requires a number of experiments to determine optimum levels. The response surface methodology (RSM) is a strong optimization procedure that can be used in optimization analysis [7,34]. The synthesis of an environment-friendly bioadsorbent without the use of toxic solvents and with high adsorption capacity to adsorb pollutants as well as with simple and convenient magnetic separation is also important; these points represent the novelty of this work.

Therefore, the purpose of this study was to investigate the equilibrium adsorption capacity of MNZ on CF/AC@Ch as a new magnetic biocomposite and optimize the process using central composite design (CCD) in RSM. Moreover, the effects of different parameters (MNZ initial concentration, pH, adsorbent dose and contact time) and their interactions for maximum adsorption analysis were investigated.

2. Materials and method

2.1. Materials

$FeCl_3\cdot 6H_2O$, $CoCl_2\cdot 6H_2O$, NaOH, activated carbon, and chitosan with purity of 99.8% were purchased from Merck-Germany. The used MNZ (99.8%) in this study was purchased from Temad Pharmaceutical Company in Iran. All the synthetic solutions of this study were prepared by twice-distilled water.

2.2. Synthesis of magnetic CF/AC@Ch biocomposite

$FeCl_3\cdot 6H_2O$ and $CoCl_2\cdot 6H_2O$ in ratio 2:1 were dissolved in 50 mL deionized water. Then, activated carbon was added to the solution and the mixture was vigorously stirred at room temperature. Afterwards, NaOH was added to the suspension within 1 h to adjust the pH at 13. Dark brown solutions were subjected to microwave irradiation. Then, the lightweight massive powder of the magnetic adsorbent formed quickly and subsequently, the black powder was isolated by a magnet washed with deionized water many times, and dried at 100°C for 24 h. The magnetic adsorbent was functionalized with chitosan. Chitosan (1 g) was added to the magnetic adsorbent under ultrasonic conditions.

2.3. Characterization of magnetic biocomposite

The crystallinity of the magnetic biocomposite was measured by X-ray diffraction (XRD). XRD patterns were recorded in the diffraction angle range $2\theta = 10–80°$ by a Rigaku ultima iv (made in Japan) using Ni-FILTERED Cu $K\alpha$ radiation. The magnetic properties of CF/AC@Ch were carried out by a vibrating-sample magnetometer (VSM) (LakeShore Cryotronics-7404) at room temperature. The field emission scanning electron microscopy (FESEM) (TESCAN mira3, Czech Republic) was used to investigate the morphology and microstructure of the magnetic biocomposite. The specific surface area and adsorption/desorption isotherm was calculated by the Brunauer-Emmett-Teller (S_{BET}) method using a specific surface analyzer (belsorp mini ii, Japan). The pore size distribution was calculated using the Barrett–Joyner–Halenda (BJH) method. To study the chemical characteristics and probable binding sites of the biocomposite, Fourier transform infrared spectroscopy (FTIR; 6300 Japan) was used.

2.4. pH point of zero charges (pHpzc)

The measurement of CF/AC@Ch pH_{pzc} was carried out by the solid addition method. First, 100 mL of the KCl solution (0.1 mol/L) was prepared at 10 different pH (2–11) values. Then, 0.01 g of the magnetic biocomposite was added to each solution. The prepared mixtures were kept at room temperature for 24 h [35]. The $pH_{initial}$ and final pH (pH_f) values of the solutions were measured by using a pH meter (Hanna). The final pH (pH_f) was plotted against the initial pH (pH_i). The intersection point of $pH_i = pH_f$ was taken as pH_{zpc}. The pH of the solutions was adjusted by NaOH and HCl 0.1 N.

2.5. Experimental design and analysis

CCD which is the most popular design in RSM was chosen to design the experiment in order to determine the effect of the independent variables on the response variable and optimize the parameters [36]. A total of 30 experiments were designed to evaluate the effect of different variables of the MNZ initial concentration (10–30 mg/l), adsorbent dose (100–1500 mg/L), pH (3–11) and contact time (5–60 min).

The results were analyzed by determining the R^2 coefficient, ANOVA and statistical response curves. The concordance of the results was investigated with linear, double-factors and quadratic models.

The quadratic equation model for predicting the optimal point is given below in Eq. (1) [36–38].

$$Y = \beta_0 + \sum_{i=1}^{k} \beta_i X_i + \sum_{i=1}^{k} \beta_{ii} X_i^2 + \sum_{i=1}^{k-1} \sum_{j=i+1}^{k} \beta_{ij} X_i X_j \quad (1)$$

where Y, β_0, β_i, β_{ii}, β_{ij}, X_i and X_j are the response (the amount of MNZ adsorption per unit mass of the adsorbent) predicted by the model, the constant coefficient, linear coefficients, quadratic coefficients, interaction coefficients and coded independent variables, respectively [38].

Design Expert 7 was used for regression and graphical analysis of the obtained data. Optimal conditions of the experiments were investigated using statistical analyses in order to obtain the optimal points of each parameter and best mathematical equation corresponding to the model.

2.6. Adsorption test

This experimental study was carried out on a laboratory scale. A stock solution of MNZ (1000 ppm) was prepared. The synthetic MNZ samples were prepared at different concentrations and the impact of the parameters affecting the process was investigated. After the adsorption process, a certain volume of the solution was taken and the magnetic biocomposite by a magnet was separated from the solution. A UV/Vis spectrophotometer (Shimadzu 1800) was used to measure the MNZ concentration in synthetic solutions with a λ_{max} of 318 nm.

The amount of MNZ adsorption per unit mass of magnetic biocomposite was calculated by Eq. (2) [12].

$$q_e = \frac{(c_0 - c_t)v}{m} \quad (2)$$

where q_e (mg/g) is the adsorption capacity, C_0 and C_t the MNZ concentration (mg/L) at time: 0 and t, v is the volume of the solution (L) and m is the mass of the used dry magnetic biocomposite (g).

A shaker with constant speed (200 rpm) was used in order to distribute the biocomposite. Then, adsorption isotherms were calculated under optimal conditions. To investigate the interference effect of pollutants in the synthetic wastewater sample, a solution with a compound of materials including glucose, sucrose, galactose, sodium chloride, calcium chloride, calcium carbonate, dipotassium hydrogen phosphate, potassium dihydrogen phosphate, magnesium sulfate, ferrous ammonium sulfate, and yeast extract in distilled water were used. Next, MNZ with a concentration of 22.35 mg/L was added to the solution. The wastewater quality was determined using the methods cited in the Standard Method for Examination of Water and Wastewater Book [39] and the extent of removal was tested under optimal conditions. The measurement of the MNZ concentration in the wastewater sample was performed by high performance liquid chromatography (HPLC, YL 9100 Waters, USA) equipped with a UV absorbance detector at the wavelength of 348 nm and a C_{18} column (250 mm × 4.6 mm, 5-µm particles size). The mobile phase was consisted of acetonitrile and deionized water (30:70; v/v), and a flow rate with 1 mL/min was used [3].

3. Results and discussion

3.1. Characterization of magnetic biocomposite adsorbent

3.1.1. The XRD analysis of magnetic biocomposite

The XRD diffraction pattern of the $CoFe_2O_4$/AC@Ch biocomposite that indicates the crystalline nature of the biocomposite is shown in Fig. 1.

The XRD pattern of the adsorbent with the crystal phase structure of the magnetic biocomposite had diffraction peaks at 2θ of 18.42° (111), 30.25° (220), 35.58° (311), 53.59° (422), 57.15° (511), 62.71° (440) and 74.14° (533). These peaks that are well indexed to the cubic spinel phase of $CoFe_2O_4$ are also in agreement with the literature data (JCPDS 96-591-0064). Diffraction peaks at 2θ = 27° (002) and 43.2° (400) [35,40] can be related to the amorphous-like structure of carbon and reveals that, even in the reaction with activated carbon and chitosan, the crystal structure of $CoFe_2O_4$ is well preserved (Fig. 1).

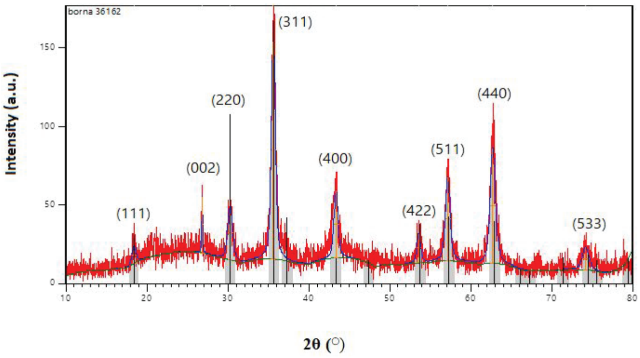

Fig. 1. The XRD analysis of the magnetic biocomposite $CoFe_2O_4$/Activated carbon @Chitosan.

3.1.2. Magnetic properties of biocomposite

The magnetic properties of the biocomposite was evaluated by a VSM at room temperature. The magnetic hysteresis loops for magnetic CF/AC@Ch are shown in Fig. 2. The high value of the magnetization curve (Ms) of the biocomposite proved a ferromagnetic character.

It can be observed that the values of coercive force, MS, and remanent magnetization were 433.02 Oe, 22.03 emu/g, and 7.16 emu/g, respectively. All these confirm sufficient magnetization for simple separation by external magnetic field. In addition, the ratio of Mr/Ms between 0 and 1 confirms the paramagnetic property of the biocomposite (Mr/Ms = 0.32). CF/AC@Ch uniformly dispersed in the MNZ solution, as shown in the inset of Fig. 2. After finishing the adsorption process, magnetic biocomposite powders were easily separated from the solution under the external magnetic field that can be recycled and reused for future runs.

3.1.3. FESEM and morphology analysis of magnetic biocomposite

Fig. 3 shows the FESEM images of the magnetic biocomposite.

The FESEM images showed the formation of nano particles with an average particle size about 30 nm. The surface morphology of the biocomposite clearly showed the formation of cobalt ferrite particles on the surface of activated carbon (Fig. 3a). After the adsorption process, no significant change was found in the adsorbent structure (Fig. 3b). This confirms that the porous structure of the biocomposite is maintained after interacting with the adsorbate.

3.1.4. FTIR analysis

The FTIR spectroscopy of the magnetic biocomposite before and after the adsorption process was carried out at 500–4000 cm^{-1}. The results are shown in Fig. 4.

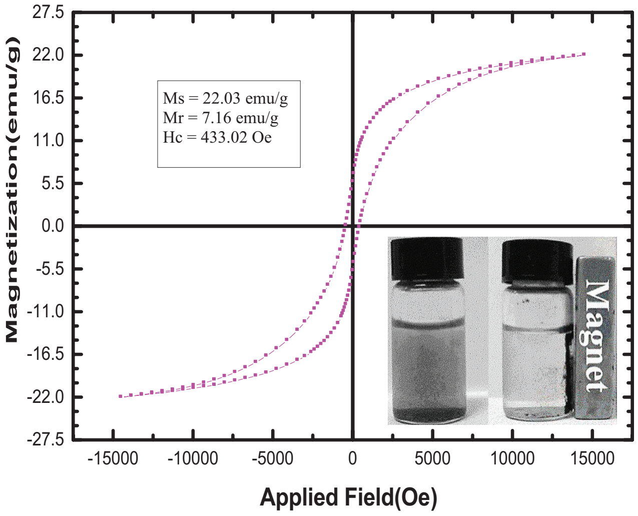

Fig. 2. The VSM magnetization curve of the magnetic biocomposite $CoFe_2O_4$/activated carbon @Chitosan.

The FTIR spectrum of the biocomposite before the adsorption process (Fig. 4a) showed a broad band from about 3400 cm^{-1} that can be related to O-H and N-H stretching bands in the chitosan. The O-H stretching can also be attributed to the presence of the adsorbed water. The strong peak observed at the wave number 591 cm^{-1} is usually related to the Fe-O bond stretching vibration of tetrahedral, which is ascribed to the characteristic peak of $CoFe_2O_4$. The peaks at the wave number 1559 cm^{-1} and about 1200 cm^{-1} can relate to N-H stretching and C-O bonds in the chitosan structure. In the FTIR spectrum, after the adsorption process (Fig. 4b), all these peaks were observed, which confirm that the adsorbent structure has not changed [25,41]. Accordingly, the absorption bands, corresponding to the stretching vibration of -NH and -OH groups, widened, weakened, and shifted to the lower wave numbers. The shift can be explained by decrease of the force constant of the OH bond as a result of the hydrogen bonding between the CF/AC@Ch biocomposite and adsorbed MNZ.

3.1.5. The BET analysis of magnetic biocomposite

The nitrogen adsorption/desorption isotherm and pore size distributions of the CF/AC@Ch biocomposite are shown in Fig. 5.

The BET analysis is the standard method for determining surface areas by measurements of the adsorption isotherm [12]. N_2 adsorption/desorption analyses showed that the specific BET surface area of the CF/AC@Ch biocomposite was 474.36 m^2/g, which was relatively high and the total pore volume ($p/p_0 = 0.987$) was obtained as 0.3745 cm^3/g. Adsorption isotherms are classified based on the strength of the interaction between the sample surface and adsorptive, and the existence or absence of pores. In this study, the isotherm was of type IV which is the characteristic of mesoporous materials. The mean pore diameter was obtained 3.157 nm by applying the BJH method. According to the International Union of Pure and Applied Chemistry classification of pores, this value indicates the CF/AC@Ch biocomposite is a mesoporous material [42]. The surface area of $CoFe_2O_4$/AC@Ch (S_{BET} = 474.36 m^2/g) was higher than the other reported by Zhu et al. for CS-m-GMCNTs (S_{BET} = 39.20 m^2/g) [33], Zhang et al. for $CoFe_2O_4$-reduced graphene oxide (S_{BET} = 169.9 m^2/g) [43], and Guo et al. for graphenes magnetic material (Fe_3O_4-GS) (S_{BET} = 62.43 m^2/g) [44].

3.2. Central composite design (CCD) experiments

The design matrix for the different experimental conditions and the equilibrium adsorption capacity of MNZ between the experimental and predicted values of the CCD model are shown in Table 1.

3.3. Choosing a model

In order to predict the results with proper power, linear, double-factor quadratic and cubic models were studied and for each model, the matching rate was examined. The results are shown in Table 2.

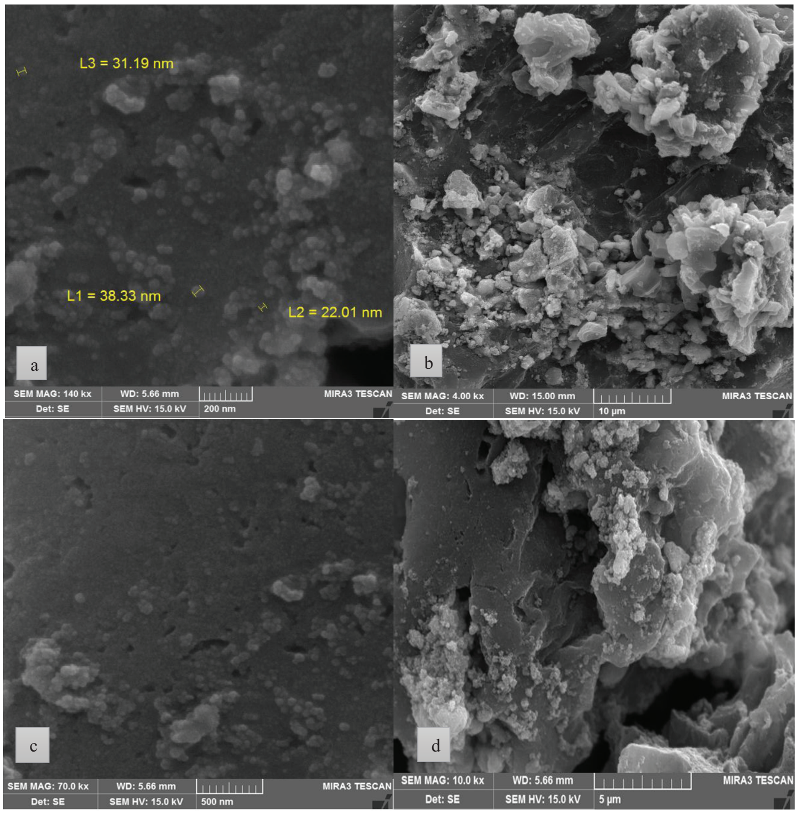

Fig. 3. FESEM images of the magnetic biocomposite $CoFe_2O_4$/activated carbon @Chitosan before (a, b) and after (c, d) the adsorption process.

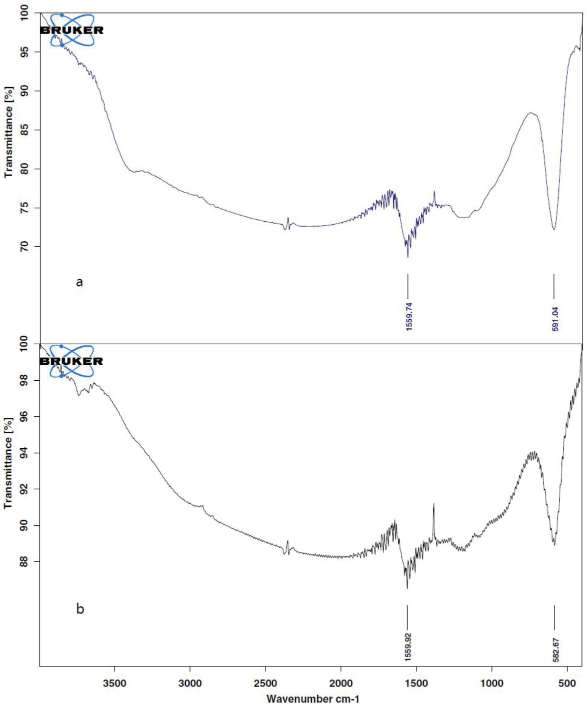

Fig. 4. The FTIR spectrum of the magnetic biocomposite $CoFe_2O_4$/activated carbon @Chitosan before (a) and after (b) the adsorption process.

The quadratic model with the highest R-squared was proposed as the best model to predict the MNZ equilibrium adsorption capacity. Therefore, this model was used to analyze the data. The quadratic model was reported as the best model in the study by Sahan et al. for Mercury(II) adsorption by a novel adsorbent mercapto-modified bentonite [12] and the study by Wan et al. for adsorption of norfloxacin onto polydopamine microspheres [7], which is consistent with the present study.

3.4. Model evaluation

ANOVA was used to evaluate the selected model and its significance test. The results are shown in Table 3.

Considering the analysis and the F-values, bioadsorbent dose (mg/L), MNZ initial concentration (mg/L), contact time (min) and pH were the most effective system variables. Factors with a p-value of less than 0.05 were considered significant [7] and kept in the model. Accordingly, Eq. (3) shows the proposed model:

$$Y = 20.98 - 1.41\,X_1 - 6.97\,X_2 + 5.01\,X_3 + 2.14\,X_4 + 1.08\,X_1X_2 + 0.41\,X_1X_4 - 1.35\,X_2X_3 - 1.07\,X_2X_4 + 0.48\,X_3X_4 - 0.47\,X_1^2 + 1.67\,X_2^2 - 0.67\,X_4^2 \quad (3)$$

where Y is the MNZ equilibrium adsorption capacity and codes X_1, X_2, X_3 and X_4 are pH, bioadsorbent dose (mg/L), MNZ initial concentrations (mg/L) and contact time (min), respectively.

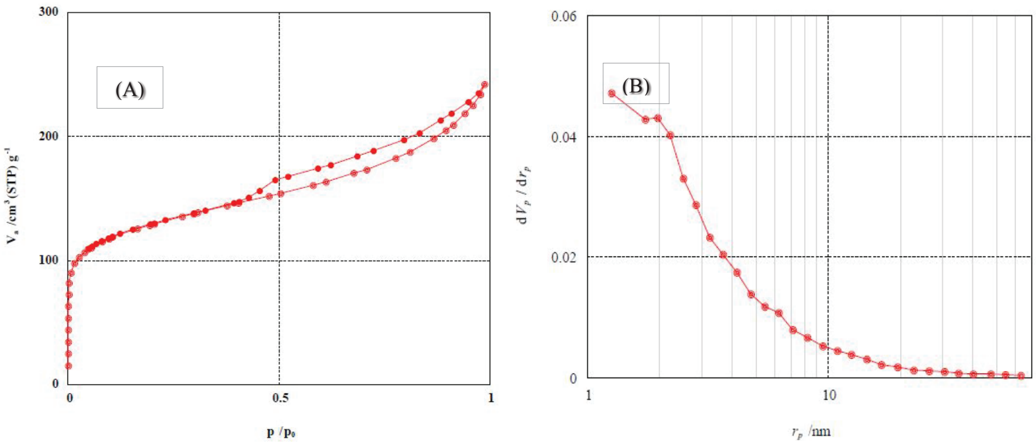

Fig. 5. The nitrogen adsorption/desorption isotherm (A) and the pore size distributions (B) of the $CoFe_2O_4$/activated carbon @Chitosan biocomposite.

Table 1
Experimental and predicted values of the MNZ equilibrium adsorption capacity

Run	pH	Adsorbent (mg L^{-1})	MNZ (mg L^{-1})	Time (min)	q_e (mg/g)	Predicted (mg/g)
1	9.00	1150.00	25.00	18.75	21.93	22.33
2	7.00	1500.00	20.00	32.50	15.99	16.29
3	3.00	800.00	20.00	32.50	11.30	11.09
4	11.00	800.00	20.00	32.50	9.70	9.35
5	9.00	1150.00	15.00	46.25	34.23	33.83
6	7.00	800.00	20.00	32.50	28.33	28.31
7	5.00	1150.00	25.00	18.75	17.43	17.18
8	9.00	450.00	25.00	18.75	15.72	15.96
9	9.00	1150.00	15.00	18.75	27.15	26.97
10	7.00	800.00	20.00	32.50	22.37	22.57
11	9.00	450.00	15.00	18.75	11.46	11.44
12	7.00	100.00	20.00	32.50	10.89	11.34
13	7.00	800.00	30.00	32.50	40.11	40.40
14	9.00	450.00	15.00	46.25	36.25	36.52
15	5.00	450.00	15.00	18.75	19.70	19.45
16	5.00	1150.00	25.00	46.25	20.31	19.87
17	5.00	450.00	25.00	46.25	21.58	21.90
18	7.00	800.00	20.00	32.50	16.59	16.28
19	9.00	450.00	25.00	46.25	42.02	41.60
20	9.00	1150.00	25.00	46.25	13.29	13.71
21	5.00	450.00	25.00	18.75	10.96	10.66
22	5.00	1150.00	15.00	46.25	30.40	30.69
23	5.00	450.00	15.00	46.25	13.87	14.03
24	7.00	800.00	20.00	60.00	22.74	22.58
25	7.00	800.00	20.00	32.50	20.22	20.98
26	5.00	1150.00	15.00	18.75	21.81	20.98
27	7.00	800.00	10.00	32.50	20.77	20.98
28	7.00	800.00	20.00	32.50	21.24	20.98
29	7.00	800.00	20.00	5.00	20.84	20.98
30	7.00	800.00	20.00	32.50	21.00	20.98

3.5. Model validation

The results of the validation and correlation coefficients of the model are shown in Table 4.

The statistical parameters selected for fitting the model include mean, standard deviation and coefficient of variation, which indicates the status of q_e data for the answer. The coefficient of variation of 2.28% represents the measurement accuracy and reliability of the tests. PRESS is the proportionality of the model in every point, for which lower values are better. Pred R-squared is the value of error. Moreover, R-squared is used to evaluate the quality of the proposed model. R-squared is the ratio of the described sum of squares to the total sum of squares, valued between 0 and 1. The closer it is to 1, the greater is the validity of the proposed model [45]. The value of R-squared in this study was equal to 0.998, indicating the high compliance of the proposed model with the MNZ equilibrium adsorption capacity.

3.6. Model optimum conditions

Derringer's desirability function was used to achieve the most favorable conditions for the MNZ equilibrium adsorption capacity [7,12]. In this method, the performance of the adsorption process is expressed by a number between 0 and 1, in which 0 represents an undesirable response and 1 indicates the desired response (Fig. 6).

The optimal conditions for the adsorption process included the bioadsorbent dose of 450 mg/L, MNZ initial concentration of 22.35 mg/L, pH of 5.02, and contact time of 46.25 min. Under these conditions, the predicted q_e of the model for MNZ adsorption was 36.89 mg/g. In the optimal conditions, the MNZ equilibrium adsorption capacity was 35.90 mg/g, indicating a strong correlation between model prediction and actual conditions.

3.7. Dimensional response surfaces and counter plots for MNZ adsorption (Y)

The response surfaces due to the effects of biocomposite dose and time, pH and time, MNZ initial concentration and

Table 2
Results of the model adequacy tested in the CCD design

Source	Sum of Squares	df	Mean Square	F Value	p-value Prob > F	Adjusted R-Squared	Predicted R-Squared	PRESS	
Linear	185.19	20	9.26	33.21	< 0.0005	0.8975	0.8625	290.47	
2FI	112.26	14	8.02	28.76	< 0.0008	0.9179	0.9136	182.51	
Quadratic	2.17	10	0.22	0.78	0.6577	0.9967	0.9931	14.49	Suggested
Cubic	9.968E-003	2	4.984E-003	0.018	0.9823	0.9972	0.9984	3.44	Aliased
Pure Error	1.39	5	0.28	–	–				

Table 3
ANOVA results of the response surface quadratic model for adsorption of MNZ on the biocomposite

Source	Sum of squares	df	Mean square	F_{Value}	P-value	Status
Model	2108.23	14	150.59	634.41	< 0.0001	Significant
X_1 (pH)	47.39	1	47.39	199.65	<0.0001	Significant
X_2 (bioadsorbent dose (mg/L))	1166.29	1	1166.29	4913.48	<0.0001	Significant
X_3 (MNZ (mg/L))	601.69	1	601.69	2534.87	< 0.0001	Significant
X_4 (time (min))	109.83	1	109.83	462.70	< 0.0001	Significant
$X_1 X_2$	18.51	1	18.51	77.96	< 0.0001	Significant
$X_1 X_3$	0.27	1	0.27	1.12	0.3070	Not Significant
$X_1 X_4$	2.69	1	2.69	11.32	0.0043	Significant
$X_2 X_3$	29.32	1	29.32	123.54	< 0.0001	Significant
$X_2 X_4$	18.45	1	18.45	77.72	< 0.0001	Significant
$X_3 X_4$	3.71	1	3.71	15.62	0.0013	Significant
X_1^2	6.14	1	6.14	25.88	0.0001	Significant
X_2^2	76.37	1	76.37	321.75	< 0.0001	Significant
X_3^2	0.16	1	0.16	0.66	0.4306	Not Significant
X_4^2	12.25	1	12.25	51.62	< 0.0001	Significant
Residual	3.56	15	0.24	–	–	–
Lack of fit	2.17	10	0.22	0.78	0.6577	Not Significant
Pure Error	1.39	5	0.28	–	–	–
Core total	2111.79	29	–	–	–	–

time on the response y (q_e) are shown in the three-dimensional (3D) response surfaces and corresponding two-dimensional (2D) contour plots (Figs. 7, 8 and 9), at central point values of other parameters.

3.7.1. Dimensional response surfaces and counter plots for effect of biocomposite dose

According to ANOVA analyses, the biocomposite dose with higher F_{Value} compared to other variables was the most effective parameter on the response y (q_e). By increasing the biocomposite dose, the amount of the adsorbed MNZ per gram of the adsorbent decreased (Figs. 7A and 7B).

In the constant concentration of MNZ, the active sites on the adsorbent surface remain unsaturated during the adsorption process. An increase at the concentration of the magnetic biocomposite caused the accumulation of the particle and thus the amount of the adsorbed MNZ per gram of the adsorbent decreased [7,12,46]. The results of previous studies indicate that the higher dose of the adsorbent results in decreased adsorption which could be ascribed to the overlying of adsorbent active sites [7,45,46]. Moreover, from the contour plot, the near-parallel lines implied that the interaction between time and bioadsorbent dose was not highly strong.

Table 4
The correlation coefficients for the response surface quadratic model

Parameter	Value	Parameter	Value
Standard deviation	0.49	R-Squared	0.9983
Mean	21.34	Adj R-Squared	0.9967
C.V.%	2.28	Pred R-Squared	0.9931
PRESS	14.49	Adeq Precision	93.589

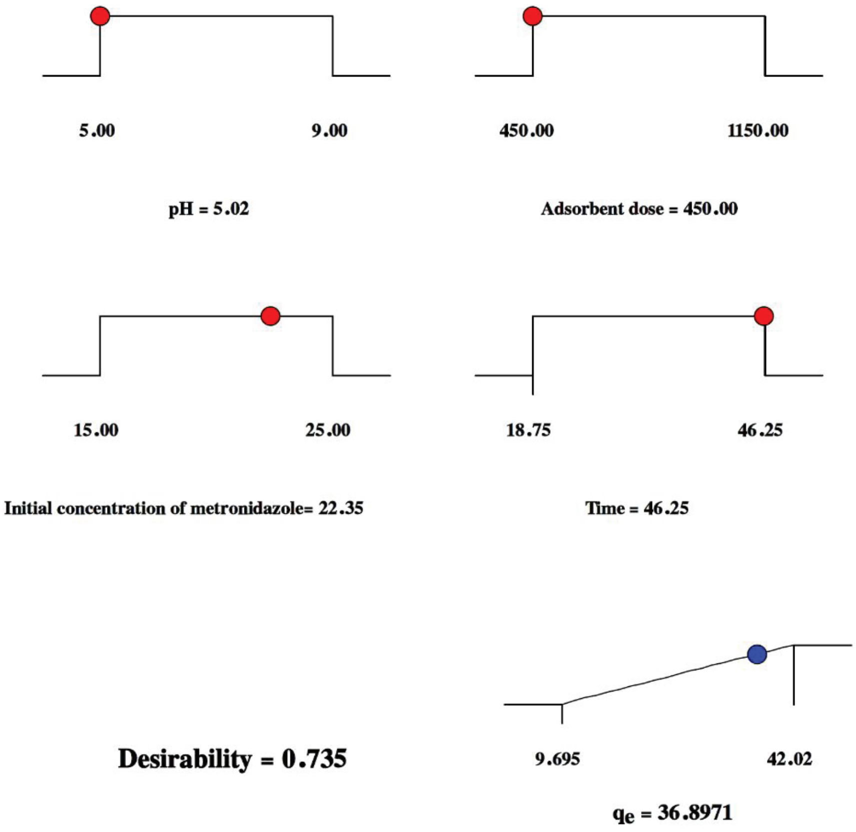

Fig. 6. Desirability ramp for MNZ adsorption process optimization.

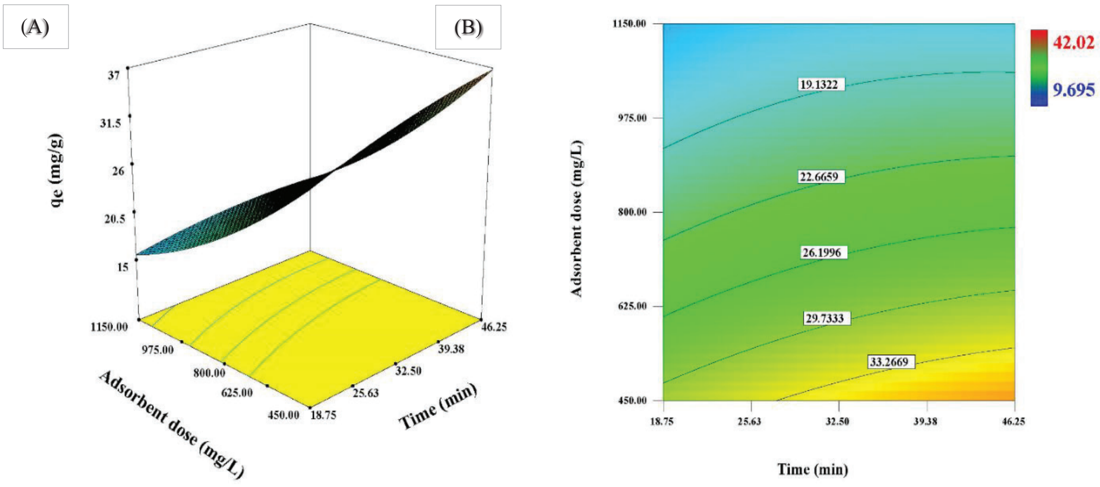

Fig. 7. The 3D response surface of the modeled MNZ adsorption capacity (A) and contour plots (B) as a function of adsorbent dose and time at central point values of other parameters.

In a study conducted by Naushad et al., the pectin based quaternary amino anion exchanger (Pc-QAE) was prepared and used for adsorption of toxic phosphate anions. They reported that the adsorption of phosphate anion increased with the increase in adsorbent dosage due to the accessibility to a large number of vacant sites [22]. Similar results are obtained from other literature [15,23,25].

3.7.2. Dimensional response surfaces and counter plots for effect of pH

The solution pH is one of the most important parameters for the wastewater treatment process. Indeed, the solution's pH affects the performance of analytes by changing the degree of ionization (pKa) and alters the superfi-

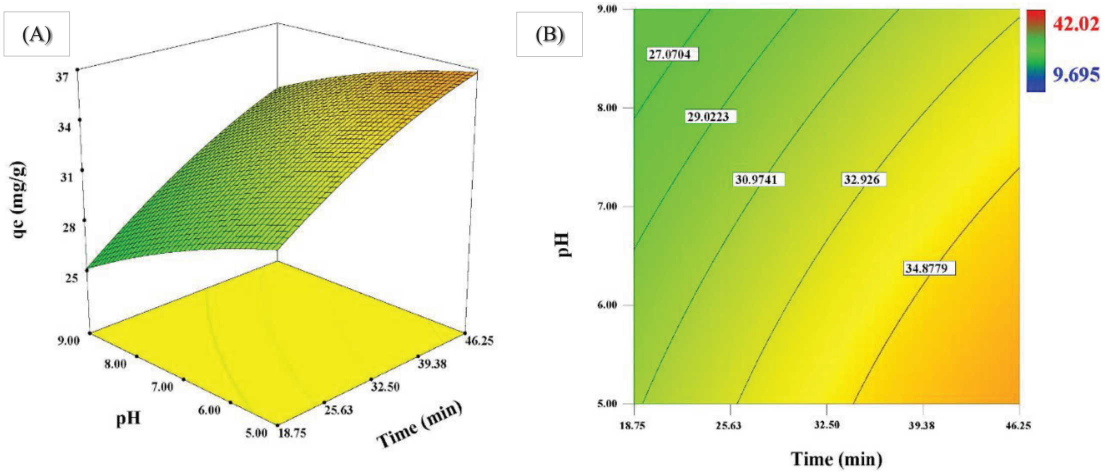

Fig. 8. The 3D response surface of the modeled MNZ adsorption capacity (A) and contour plots (B) as a function of pH and time at central point values of other parameters.

cial coupling sites of the adsorption [12,46]. The CF/AC@Ch behavior over the pH range of 5–9 was presented in the 3D response surfaces and corresponding 2D contour plots (Figs. 8A and B); it is easily realized that the optimum MNZ adsorption was achieved at pH = 5.

By increasing pH from 5 to 9, the uptake of MNZ ions decreased. The CCD model predicted that the highest adsorption of MNZ should be at pH = 5.02 as the optimum value. The effect of pH may be explained in terms of pH_{zpc} of the adsorbent (the pH_{zpc} of the CF/AC@Ch calculated by the solid addition method was 6.4 [35]. At pH below $pH_{zpc,}$ the surface charge of the CF/AC@Ch was positive, thereby increasing the chance of adsorption of MNZ ions [12,35]. This result agrees with those of the previous studies [12]. The results of previous studies indicated that, where pH = 5, amino groups in chitosan on the surface of the biocomposite were protonated and adsorbed MNZ ions [47]. At pH above pH_{zpc}, the surface of the CF/AC@Ch became less positive or more negative [35]. As a result, the repulsion between the interfaces increased in the solution while the electrostatic attraction decreased [35]. On the other hand, high pHs resulted in higher concentrations of OH^- in the solution, inhibiting scattering of MNZ ions and thereby decreasing the chance of their adsorption [12,47]. Moreover, from the contour plot, the near-parallel lines implied that interaction between time and pH was weak.

3.7.3. Dimensional response surfaces and counter plots for effect of MNZ initial concentration

The response surfaces due to the effects of the MNZ initial concentration and time on the response y (q_e) were shown in the 3D response surfaces and corresponding 2D contour plots (Figs. 9A and B), at central point values of other parameters.

At the constant level of the magnetic biocomposite, with increasing the MNZ initial concentration, the equilibrium adsorption capacity (q_e) value increased. The initial concentration of MNZ provided an important driving force of concentration gradient to overcome the resistance force of the mass transfer of MNZ between the solution and solid phase [12,45,46]. Moreover, from the contour plot, the near-parallel lines implied that interaction between time and pH was almost weak.

Almost all the literature reported that the initial concentration of pollutants strongly affected the adsorption of adsorbate ions on the adsorbent. With the increase in the initial concentration of pollutants, the uptake rate of adsorbate ions increase, due to the increase in interactions between adsorbate molecules and the adsorbent [14,17,24,25].

In a study conducted by Marrakchi et al. for the adsorption of methylene blue (MB), a mesoporous-activated carbon was prepared from chitosan flakes (CS) via single-step sodium hydroxide activation. The results of their study showed that with the increase of the MB initial concentration from 25 to 400 mg/L, the adsorbed amount of the MB dye increased from 27.35 mg/g to 128.90 mg/g [25]. Similar results were obtained from the studies of Danish et al. [26], Khanday et al. [24], and Marrakchi et al. [23]. The results of these researches are congruent with the result of our research.

3.8. Adsorption isotherm studies

Adsorption isotherms are mathematical models that describe the interaction of adsorbate species with the adsorbent. Langmuir isotherm is based on the assumptions that adsorption occurs in a series of special homogeneous sites on the outer surface of the adsorbent, all sites are equivalent, only mono-layer adsorption occurs and there is no interaction between adsorbate molecules on adjacent sites [22].

The linear equation of the Langmuir isotherm is presented as follows [14,25]:

$$\frac{C_e}{q_e} = \frac{1}{K_L q_m} + \frac{C_e}{q_m} \tag{4}$$

where q_e is the quantity of the adsorbate adsorbed per unit weight of the adsorbent at equilibrium (mg/g), C_e is the concentration of the adsorbate at equilibrium in the solution after adsorption (mg/L), q_m is the maximum adsorp-

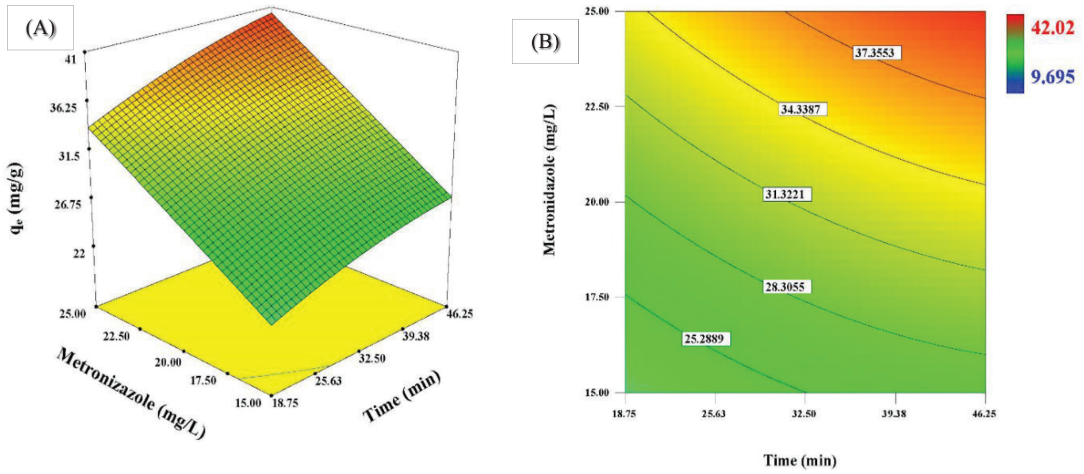

Fig. 9. The 3D response surface of the modeled MNZ adsorption capacity (A) and contour plots (B) as a function of MNZ initial concentration and time at central point values of other parameters.

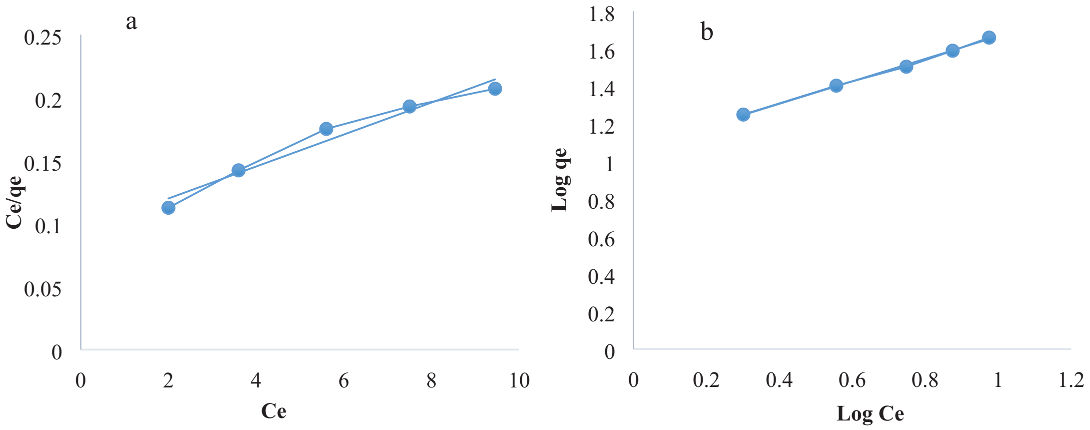

Fig. 10. The Langmuir isotherm (a) and the Freundlich isotherm (b) for the MNZ adsorption under optimal conditions (pH: 5.02, adsorbent dose: 450 mg/L and contact time: 46.25 min).

tion capacity (mg/g) and b is the Langmuir adsorption equilibrium constant (L/mg) [14,25].

The essential characteristic of the Langmuir isotherm is expressed on the basis of a dimensionless constant referred to as an equilibrium parameter or separation factor (R_L) and can be expressed as follows [17]:

$$R_L = \frac{1}{(1 + K_L C_0)} \tag{5}$$

where C_0 (mg/L) is the initial concentration and K_L (L/mg) is the constant related to the energy of adsorption (the Langmuir constant). The value of R_L indicates the adsorption nature to be either unfavorable ($R_L > 1$), irreversible ($R_L = 0$), favorable ($0 < R_L < 1$) or linear ($R_L = 1$) [17].

The Freundlich isotherm is an empirical expression based on adsorption on a heterogeneous surface with a non-uniform distribution of the adsorption heat on the surface. This model estimates the sorption intensity of the adsorbent towards the adsorbate [17,25].

The linear equation of the Freundlich isotherm is presented as Eq. (6) [25]:

$$\log q_e = \log K_f + 1/\mathrm{n}\ Log\ C_e \tag{6}$$

where K_F is the Freundlich constants related to the adsorption capacity and $1/n$ is the adsorption intensity (or heterogeneity factor). In the Freundlich isotherm model, a value for $1/n < 1$ infers stronger interaction between the adsorbate and adsorbent, which indicates a favorable sorption process. If $1/n > 1$, cooperative adsorption is indicated [17,25].

The plots of the Langmuir and Freundlich isotherms for the MNZ adsorption are shown in Fig. 10 while the parameters and correlation coefficients of the isotherms are presented in Table 5.

The results presented in Table 5 indicated that the adsorption process followed the Freundlich isotherm ($R^2 = 0.9981$).

3.9. Interference effect of present pollutants in synthetic wastewater

The results of quality analysis of the synthetic wastewater sample, equilibrium adsorption capacity and removal efficiency of MNZ under optimal conditions are shown in Table 6.

Table 5
The Langmuir and Freundlich isotherm parameters (adsorbent: 450 mg/L, contact time: 46.25 min, pH: 5.01, and initial concentration of MNZ: 10, 15, 20, 25, 30 mg/L)

	Freundlich Isotherm			Langmuir Isotherm			
$CoFe_2O_4$/Activated carbon@Chitosan	R^2	$K_f[(mg/g)(1/mg)]$	$1/n$	R^2	R_L	$q_m[(mg/g)$	$K_L\,(L/mg)$
	0.9981	11.656	0.599	0.9637	0.427	78.740	0.134
					0.332		
					0.271		
					0.229		
					0.199		

Table 6
Quality analysis of the synthetic wastewater sample

Paramaters	Results
pH	6
COD (mg/L)	450
BOD (mg/L)	210
TSS (mg/L)	20
TDS (mg/L)	115
EC (µs/cm)	1520
Turbidity (NTU)	8
Sulphat (mg/L)	5
MNZ concentration (mg/L)	22.35
MNZ removal efficiency (%)	55
Equilibrium adsorption capacity (q_e)	21.5

The interference effect of present pollutants in the synthetic wastewater sample was investigated. As can be observed in Table 6, compounds such as dissolved organic matter, suspended organic matter, sulfate anions and other dissolved chemical compounds in the wastewater sample competed with MNZ molecules to adsorb the magnetic biocomposite. The molecules that were smaller and had greater tendency to form bonds with hydroxyl groups (OH) occupied the active sites of the biocomposite surface. Therefore, the equilibrium adsorption capacity of MNZ declined from 35.90 mg/g in the pure solution of MNZ to 21.5 mg/g in the wastewater sample.

4. Conclusion

In this study, CF/AC@Ch was prepared by microwave irradiation co-assisted by ultrasonic waves in water without the use of toxic solvents, which was used as a magnetic biocomposite and characterized by XRD, FESEM, VSM, FTIR, and BET analyses. The pH_{ZPC} value of the biocomposite was estimated to be 6.4 by the solid addition method. RSM with CCD design was applied for optimizing and modeling the adsorption capacity of MNZ from an aqueous solution. The optimal predicted adsorption capacity (q_e) of MNZ onto the CF/AC@Ch was obtained 36.897 mg/g. The S_{BET} surface area of the adsorbent was 474.36 m^2/g, which was relatively high. The mean pore diameter was obtained 3.157 nm by applying the BJH method. Effective factors in the system were optimized by RSM. The quadratic model obtained a removal efficiency rate with a desirable fitting degree. The CF/AC@Ch as a new biocomposite can be utilized as an environment friendly bioadsorbent for the removal of antibiotics from aqueous solutions due to its high adsorption capacity, as well as its simple and convenient magnetic separation.

Acknowledgements

This research was conducted at the Environmental Health Engineering Research Center and sponsored by the Vice-Chancellor for Research and Technology of the Kerman University of Medical Sciences. A note of appreciation is expressed here to the Vice-Chancellor and all the university staff who provided assistance to make this study possible.

References

[1] M. Malakootian, M. Yaseri, M. Faraji, Removal of antibiotics from aqueous solutions by nanoparticles: a systematic review and meta-analysis, Environ. Sci. Pollut. Res., 26 (2019) 8444–8458.

[2] F.N. Chianeh, J.B. Parsa, Electrochemical degradation of metronidazole from aqueous solutions using stainless steel anode coated with SnO_2 nanoparticles: experimental design, J. Taiwan Inst. Chem. Eng., 59 (2016) 424–432.

[3] W. Cheng, M. Yang, Y. Xie, B. Liang, Z. Fang, E.P. Tsang, Enhancement of mineralization of metronidazole by the electro-Fenton process with a Ce/SnO_2–Sb coated titanium anode, Chem. Eng. J., 220 (2013) 214–220.

[4] A. Nasiri, F. Tamaddon, M.H. Mosslemin, M. Amiri Gharaghani, A. Asadipour, New magnetic nanobiocomposite $CoFe_2O_4$@methycellulose: facile synthesis, characterization, and photocatalytic degradation of metronidazole, J. Mater. Sci., (2019) Article in Press.

[5] M. Malakootian, N. Olama, A. Nasiri, Photocatalytic degradation of metronidazole from aquatic solution by TiO_2-doped Fe^{3+} nano-photocatalyst, Int. J. Environ. Sci. Technol., (2017) 1–10.

[6] M. Malakootian, A. Nasiri, A. Asadipour, E. Kargar, Facile and green synthesis of $ZnFe_2O_4$@CMC as a new magnetic nanophotocatalyst for ciprofloxacin degradation from aqueous media, Process Saf. Environ. Prot., (2019) Article in Press.

[7] Y. Wan, X. Liu, P. Liu, L. Zhao, W. Zou, Optimization adsorption of norfloxacin onto polydopamine microspheres from aqueous solution: Kinetic, equilibrium and adsorption mechanism studies, Sci. Total Environ., 639 (2018) 428–437.

[8] T. Yi, Study on Pharmaceutic wastewaer treatment with SBR process, China Biogas, 1 (2002) 002.

[9] M.Y. Badi, A. Azari, H. Pasalari, A. Esrafili, M. Farzadkia, Modification of activated carbon with magnetic Fe_3O_4 nanoparticle composite for removal of ceftriaxone from aquatic solutions, J. Mol. Liq., 261 (2018) 146–154.

[10] M. Malakootian, M. Amiri Gharghani, A. Dehdarirad, M. Khatami, M. Ahmadian, M.R. Heidari, H. Mahdizadeh, ZnO nanoparticles immobilized on the surface of stones to study the removal efficiency of 4-nitroaniline by the hybrid advanced oxidation process (UV/ZnO/O_3), J. Mol. Struct., 1176 (2019) 766–776.

[11] M. Malakootian, M.H. Ehrampoush, H. Mahdizadeh, A. Golpayghani, Comparison studies of raw and oxidized multi-walled carbon nanotubes H_2SO_4/HNO_3 to remove para-nitroaniline from aqueous solution, J. Water Chem. Technol., 40(6) (2018) 327–333.

[12] T. Şahan, F. Erol, Ş. Yılmaz, Mercury (II) adsorption by a novel adsorbent mercapto-modified bentonite using ICP-OES and use of response surface methodology for optimization, Microchem. J., 138 (2018) 360–368.

[13] A. Kumar, A. Kumar, G. Sharma, M. Naushad, F.J. Stadler, A.A. Ghfar, P. Dhiman, R.V. Saini, Sustainable nano-hybrids of magnetic biochar supported g-C_3N_4/$FeVO_4$ for solar powered degradation of noxious pollutants-Synergism of adsorption, photocatalysis and photo-ozonation, J. Clean. Prod., 165 (2017) 431–451.

[14] G. Sharma, A. Kumar, K. Devi, S. Sharma, M. Naushad, A.A. Ghfar, T. Ahamad, F.J. Stadler, Guar gum-crosslinked-Soya lecithin nanohydrogel sheets as effective adsorbent for the removal of thiophanate methyl fungicide, Int. J. Biol. Macromol., 114 (2018) 295–305.

[15] G. Sharma, B. Thakur, M. Naushad, A. Kumar, F.J. Stadler, S.M. Alfadul, J.T. Mola, Applications of nanocomposite hydrogels for biomedical engineering and environmental protection, Environ. Chem. Lett., 16 (2018) 113–146.

[16] G. Sharma, M. Naushad, D. Pathania, A. Mittal, G. El-Desoky, Modification of Hibiscus cannabinus fiber by graft copolymerization: Application for dye removal, Desal. Water Treat., 54 (2015) 3114–3121.

[17] M. Naushad, S. Vasudevan, G. Sharma, A. Kumar, Z. ALOthman, Adsorption kinetics, isotherms, and thermodynamic studies for Hg^{2+} adsorption from aqueous medium using alizarin red-S-loaded amberlite IRA-400 resin, Desal. Water Treat., 57 (2016) 18551–18559.

[18] A. Kumar, A. Kumar, G. Sharma, H. Alaâ, M. Naushad, A.A. Ghfar, C. Guo, F.J. Stadler, Biochar-templated g-C_3N_4/$Bi_2O_2CO_3$/$CoFe_2O_4$ nano-assembly for visible and solar assisted photo-degradation of paraquat, nitrophenol reduction and CO_2 conversion, Chem. Eng. J., 339 (2018) 393–410.

[19] M. Naushad, T. Ahamad, G. Sharma, H. Ala'a, A.B. Albadarin, M.M. Alam, Z.A. ALOthman, S.M. Alshehri, A.A. Ghfar, Synthesis and characterization of a new starch/SnO_2 nanocomposite for efficient adsorption of toxic Hg^{2+} metal ion, Chem. Eng. J., 300 (2016) 306–316.

[20] G. Sharma, A. Kumar, M. Naushad, A. García-Peñas, H. Ala'a, A.A. Ghfar, V. Sharma, T. Ahamad, F.J. Stadler, Fabrication and characterization of Gum ara-bic-cl-poly (acrylamide) nanohydrogel for effective adsorption of crystal violet dye, Carbohydr. Polym., 202 (2018) 444–453.

[21] M. Naushad, Surfactant assisted nano-composite cation exchanger: Development, characterization and applications for the removal of toxic Pb^{2+} from aqueous medium, Chem. Eng. J., 235 (2014) 100–108.

[22] M. Naushad, G. Sharma, A. Kumar, S. Sharma, A.A. Ghfar, A. Bhatnagar, F.J. Stadler, M.R. Khan, Efficient removal of toxic phosphate anions from aqueous environment using pectin based quaternary amino anion exchanger, Int. J. Biol. Macromol., 106 (2018) 1–10.

[23] F. Marrakchi, W. Khanday, M. Asif, B. Hameed, Cross-linked chitosan/sepiolite composite for the adsorption of methylene blue and reactive orange 16, Int. J. Biol. Macromol., 93 (2016) 1231–1239.

[24] W. Khanday, M. Asif, B. Hameed, Cross-linked beads of activated oil palm ash zeolite/chitosan composite as a bio-adsorbent for the removal of methylene blue and acid blue 29 dyes, Int. J. Biol. Macromol., 95 (2017) 895–902.

[25] F. Marrakchi, M. Ahmed, W. Khanday, M. Asif, B. Hameed, Mesoporous-activated carbon prepared from chitosan flakes via single-step sodium hydroxide activation for the adsorption of methylene blue, Int. J. Biol. Macromol., 98 (2017) 233–239.

[26] M. Danish, W.A. Khanday, R. Hashim, N.S.B. Sulaiman, M.N. Akhtar, M. Nizami, Application of optimized large surface area date stone (Phoenix dactylifera) activated carbon for rhodamin B removal from aqueous solution: Box-Behnken design approach, Ecotoxicol. Environ. Saf., 139 (2017) 280–290.

[27] K. Karthik, S. Dhanuskodi, C. Gobinath, S. Prabukumar, S. Sivaramakrishnan, Ultrasonic-assisted CdO–MgO nanocomposite for multifunctional applications, Mater. Technol. 34 (2019) 403–414.

[28] S. Martinez–Vargas, A.I. Martínez, E.E. Hernández–Beteta, O.F. Mijangos–Ricardez, V. Vázquez–Hipólito, C. Patiño-Carachure, J. López–Luna, As(III) and As(V) adsorption on manganese ferrite nanoparticles, J. Mol. Struct., 1154 (2018) 524–534.

[29] K. Koc, E. Alveroglu, Adsorption and desorption studies of lysozyme by Fe_3O_4–polymer nanocomposite via fluorescence spectroscopy, J. Mol. Struct., 1089 (2015) 66–72.

[30] V. Revathi, K. Karthik, Microwave assisted CdO–ZnO–MgO nanocomposite and its photocatalytic and antibacterial studies, J. Mater. Sci. Mater. Electron., 29 (2018) 18519–18530.

[31] K. Karthik, M. Madhukara Naik, M. Shashank, M. Vinuth, V. Revathi, Microwave-Assisted ZrO_2 Nanoparticles and its photocatalytic and antibacterial studies, J. Clust. Sci., 30 (2019) 311–318.

[32] Q. Zhao, H. Zhao, L. Yan, M. Bi, Y. Li, Y. Zhou, Z. Song, T. Jiang, Efficient removal of Pb (II) from aqueous solution by $CoFe_2O_4$/Graphene oxide nanocomposite: Kinetic, isotherm and thermodynamic, J. Nanosci. Nanotechnol., 17 (2017) 3951–3958.

[33] H. Zhu, Y. Fu, R. Jiang, J. Yao, L. Liu, Y. Chen, L. Xiao, G. Zeng, Preparation, characterization and adsorption properties of chitosan modified magnetic graphitized multi-walled carbon nanotubes for highly effective removal of a carcinogenic dye from aqueous solution, Appl. Surf. Sci., 285 (2013) 865–873.

[34] V. Javanbakht, S.M. Ghoreishi, Application of response surface methodology for optimization of lead removal from an aqueous solution by a novel superparamagnetic nanocomposite, Adsorp. Sci. Technol., 35 (2017) 241–260.

[35] D. Datta, Ö. Kerkez Kuyumcu, Ş.S. Bayazit, M. Abdel Salam, Adsorptive removal of malachite green and Rhodamine B dyes on Fe_3O_4/activated carbon composite, J. Dispers. Sci. Technol., 38 (2017) 1556–1562.

[36] J. Sharma, P. Anand, V. Pruthi, A.S. Chaddha, J. Bhatia, B. Kaith, RSM-CCD optimized adsorbent for the sequestration of carcinogenic rhodamine-B: Kinetics and equilibrium studies, Mater. Chem. Phys., 196 (2017) 270–283.

[37] N. Mehrabi, M. Soleimani, H. Sharififard, M. Madadi Yeganeh, Optimization of phosphate removal from drinking water with activated carbon using response surface methodology (RSM), Desal. Water Treat., 57 (2016) 15613–15618.

[38] H. Kalavathy, I. Regupathi, M.G. Pillai, L.R. Miranda, Modelling, analysis and optimization of adsorption parameters for H_3PO_4 activated rubber wood sawdust using response surface methodology (RSM), Colloids Surf. B Biointerfaces., 70 (2009) 35–45.

[39] APHA, AWWA, WEF, Standard Methods for the Examination of Water and Wastewater, ed. 20. USA: APHA, AWWA, WEF; 1998, p. 3–54, 3–5.

[40] W. Deligeer, Y. Gao, S. Asuha, Adsorption of methyl orange on mesoporous γ-Fe_2O_3/SiO_2 nanocomposites, Appl. Surf. Sci., 257 (2011) 3524–3528.

[41] B.C. Smith, Fundamentals of Fourier transform infrared spectroscopy: CRC press; 2011.

[42] M. Thommes, K. Kaneko, A.V. Neimark, J.P. Olivier, F. Rodriguez-Reinoso, J. Rouquerol, K. Sing, Physisorption of gases, with special reference to the evaluation of surface area and pore size distribution (IUPAC Technical Report), Pure Appl. Chem., 87 (2015) 1051–1059.

[43] Y. Zhang, L. Yan, W. Xu, X. Guo, L. Cui, L. Gao, Q. Wei, B. Du, Adsorption of Pb (II) and Hg (II) from aqueous solution using magnetic $CoFe_2O_4$-reduced graphene oxide, J. Mol. Liq., 191 (2014) 177–182.

[44] X. Guo, B. Du, Q. Wei, J. Yang, L. Hu, L. Yan, W. Xu, Synthesis of amino functionalized magnetic graphenes composite material and its application to remove Cr (VI), Pb (II), Hg (II), Cd (II) and Ni (II) from contaminated water, J. Hazard. Mater., 278 (2014) 211–220.

[45] M.E.M. Ali, H. Abdelsalam, N.S. Ammar, H.S. Ibrahim, Response surface methodology for optimization of the adsorption capability of ball-milled pomegranate peel for different pollutants, J. Mol. Liq., 250 (2018) 433–445.

[46] H. Zhu, Y. Fu, R. Jiang, J. Yao, L. Xiao, G. Zeng, Optimization of copper (II) adsorption onto novel magnetic calcium alginate/maghemite hydrogel beads using response surface methodology, Ind. Eng. Chem. Res., 53 (2014) 4059–4066.

[47] N. Rahbar, A. Jahangiri, S. Boumi, M.J. Khodayar, Mercury removal from aqueous solutions with chitosan-coated magnetite nanoparticles optimized using the box-behnken design, Jundishapur. J. Nat. Pharm. Prod., 9 (2014) e15913.